Optical pulse shaper with integrated slab waveguide for arbitrary waveform generation using optical gradient force*

Liao Sha-Sha(廖莎莎), Min Shu-Cun(闵书存), and Dong Jian-Ji(董建绩)†

Wuhan National Laboratory for Optoelectronics, Huazhong University of Science and Technology, Wuhan 430074, *China*

(Received 8 May 2014; revised manuscript received 10 June 2014; published online 10 October 2014)

Integrated optical pulse shaper opens up possibilities for realizing the ultra high-speed and ultra wide-band linear signal processing with compact size and low power consumption. We propose a silicon monolithic integrated optical pulse shaper using optical gradient force, which is based on the eight-path finite impulse response. A cantilever structure is fabricated in one arm of the Mach–Zehnder interferometer (MZI) to act as an amplitude modulator. The phase shift feature of waveguide is analyzed with the optical pump power, and five typical waveforms are demonstrated with the manipulation of optical force. Unlike other pulse shaper schemes based on thermo–optic effect or electro–optic effect, our scheme is based on a new degree of freedom manipulation, i.e., optical force, so no microelectrodes are required on the silicon chip, which can reduce the complexity of fabrication. Besides, the chip structure is suitable for commercial silicon on an insulator (SOI) wafer, which has a top silicon layer of about 220 nm in thickness.

Keywords: pulse shaping, arbitrary waveform generation, optical grant force

PACS: 42.65.Re, 42.79.Gn, 42.50.Wk, 42.79.Sz **DOI:** 10.1088/1674-1056/23/12/124211

1. Introduction

Optical arbitrary waveform generation (OAWG) plays a critical role in generating ultra-wide band (UWB) signal,[1,2] all-optical temporal differentiator[3,4] and integrator, high speed communication, pulse radar,[5] and signal processing.[6] A plethora of schemes about OAWGs using discrete or integrated photonic devices have been reported in recent years. Widely adopted approaches by discrete devices were reported in which gratings[7–16] were used as spectral dispersers and spatial light modulators (SLMs)[7–9,11–13] or fiber Bragg gratings (FBGs)[10,14–16] served as amplitude modulators. Although these schemes have shown flexibility in reconfiguration, the use of discrete devices may make the system bulky, consume more power, and even become unstable.[17] Therefore the integrated schemes are very desirable due to their compactness, low power consumption, and scalability with electronics. In the proposed integrated schemes, arrayed waveguide gratings[17–20] act as spectral dispersers, and thermally-tuned Mach–Zehnder modulators (MZM)[17,19]/microrings[21] or electro absorption modulators (EAMs)[18,20] provide amplitude modulation. But the requirements of metal electrodes or the processing of p-type and n-type doping make the chip fabrication expensive and complex.

Optical gradient force in an integrated waveguide has been widely investigated as a new degree of freedom in recent years. Optical force can cause a waveguide to deform, the effective index varies and further induces the phase variation.[22] The two typical structures of optical gradient force are double clamp and cantilever. For example, a π-phase variation has been obtained with optical pump power of milliwatt level by both structures.[22] But the heights of the waveguide and nanostring were usually more than 500 nm.[22,23] So this device design is not suitable for commercial silicon on insulator (SOI) wafer, which has a top silicon layer of about 220 nm or 340 nm in thickness.

In this paper, we propose a silicon-integrated optical pulse shaper based on finite impulse response (FIR) using optical gradient force with sub-milliwatt level pump power to realize the amplitude modulation. The pulse shaper is on an SOI wafer (220-nm thick silicon on 2-μm-thick silica) and etched into a thickness of 220 nm to realize a slab waveguide. We investigate the phase variation with the pump power and take the deviation caused by incident light into consideration. Then we demonstrate five typical waveforms using this scheme. Compared with other pulse shapers based on thermo–optic effect or electro–optic effect, our scheme is based on a new degree of freedom manipulation, i.e., optical force, so no microelectrodes are required on the silicon chip, which simplifies the fabrication process. Besides, the chip structure is suitable for commercial silicon on insulator (SOI) wafer, which has a top silicon layer of about 220 nm in thickness.

*Project supported by the National Natural Science Foundation of China (Grant Nos. 60901006 and 11174096), the National Basic Research Program of China (Grant No. 2011CB301704), the Program for New Century Excellent Talents in Ministry of Education of China (Grant No. NCET-11-0168), and the Foundation for the Author of National Excellent Doctoral Dissertation of China (Grant No. 201139).

†Corresponding author. E-mail: jjdong@mail.hust.edu.cn

© 2014 Chinese Physical Society and IOP Publishing Ltd

2. Principle and result

The integrated optical pulse shaper is based on eight-tap finite impulse response (FIR), and each tap has an amplitude modulator which is realized by a Mach–Zehnder interferometer (MZI) with one arm phase-modulated by optical force. From the proposed scheme we know the structures of cantilever and double clamp can both be used for phase shifting with optical gradient forces, but cantilever structure has more deformations and more phase variations when the same pump power is launched into the waveguide.[22] Therefore, we choose the cantilever structure to build our amplitude modulators. The three-dimensional (3D) schematic diagram and cross section of the cantilever structure are shown in Figs. 1(a) and 1(b).

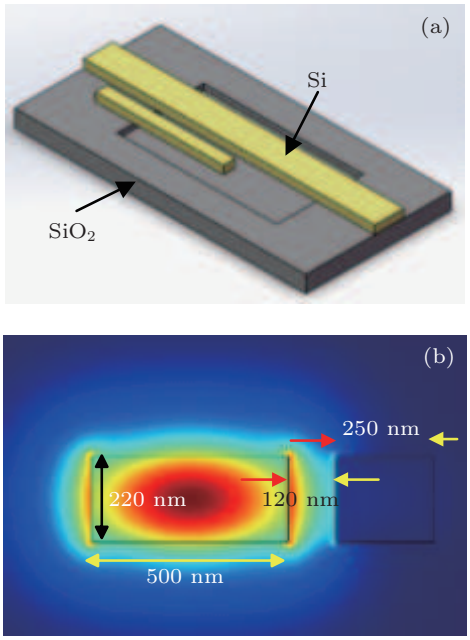


Fig. 1. (color online) (a) 3D schematic plot and (b) cross section of the cantilever and fundamental mode distribution.

The SOI is a 220-nm-thick silicon structure on a 2-μm-thick silica. The heights of the waveguide and nanostring are 220 nm and their widths are 500 nm and 250 nm respectively. And the nanostring is non-mode carrying due to its small cross-sectional area. So the light will always transport along the waveguide. The gap between the waveguide and nanostring is 120 nm when there is no incidence of pump light. The length of the nanostring is 90 μm.

As we choose slab waveguides to build our cantilever structure, the fabrication process is simpler than that with using ridge waveguides. E-beam lithography and inductively coupled plasma (ICP) can be used to form all waveguides (including the nanostrings), and then HF-vapor selectively undercut the buried oxide layer to realize the cantilever structure.

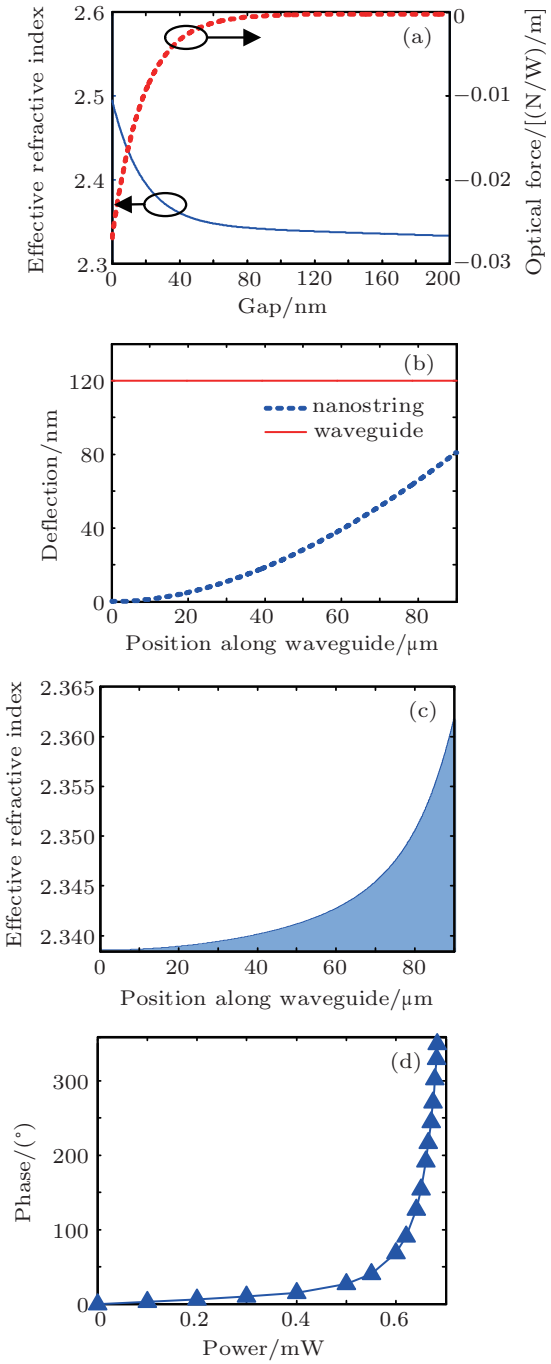


Fig. 2. (color online) (a) Variations of effective refractive index (the solid line) and optical force (the dash line) with gap size, variations of (b) deflection of the nanostring and (c) effective refractive index with position along the waveguide, (d) variation of phase with pump power.

The wavelength of pump light is 1480 nm and that of signal is 1550 nm. The gradient optical force near a waveguide can be described by[22,24,25]

$$\frac{F}{LP} = \frac{1}{C}\frac{\partial n_{\text{eff}}}{\partial d}, \tag{1}$$

where F is the optical force, L the length of the cantilever structure, P the pump power launched into the waveguide, n_{eff} the effective refractive index, and d the gap between the waveguide and the nanostring. According to the Euler–Bernoulli beam theory, the deflection of the nanostring can be described by

$$\frac{\mathrm{d}^4 u}{\mathrm{d}z^4} = \frac{12}{Et^2} \cdot \frac{F}{LP} \cdot \frac{P}{A}, \tag{2}$$

where $E = 1.31 \times 10^{11}$ Pa is the silicon's Young's modulus, $A = 5.5 \times 10^4$ nm^2 the nanostring cross-section area, and $t = 250$ nm the nanostring width. Combining Eqs. (1) and (2), we can obtain the deflection of the nanostring. Figure 2(a) shows effective refractive index (solid line) and optical force (dashed line) each as a function of gap size. Figure 2(b) shows the deflection variations of nanostring and waveguide with position along the waveguide when the pump power is 0.45 mW. We can see the largest deflection of the nanostring is about 80 nm while the deflection of waveguide is almost unchanged. Figure 2(c) shows the variation of effective refractive index with position along the waveguide propagation, owing to the nanostring's deflection. We can calculate the total phase variation from the following equation:

$$\phi = \frac{\int n_{\mathrm{eff}}(z)\,\mathrm{d}z - n_{\mathrm{eff}}(d_0) \cdot L}{\lambda} \times 360^\circ. \tag{3}$$

Figure 2(d) shows the total phase shift with different pump powers. We can see the phase shift of 360° is obtained with a low pump power of only 0.6838 mW. Then we can build an amplitude modulator by using an MZI where one arm is the cantilever structure adjusted by optical pump power.

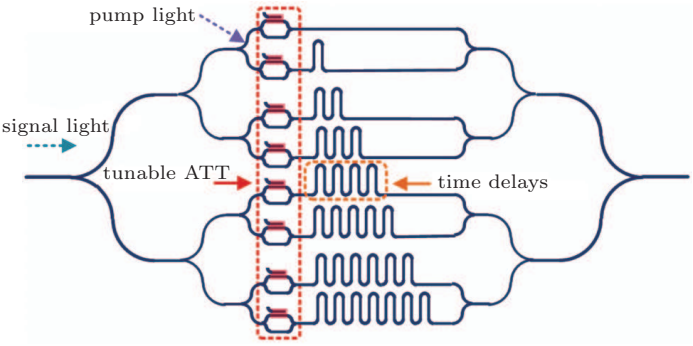


Fig. 3. (color online) Schematic diagram of the pulse shaper.

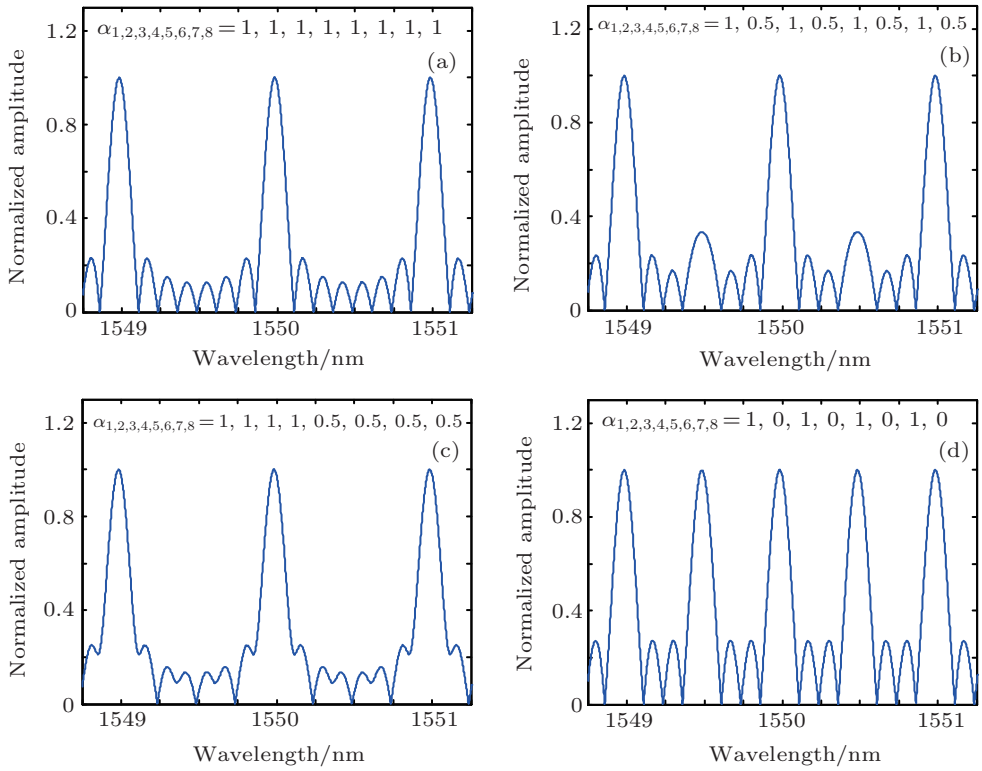


Fig. 4. (color online) Simulated spectra of the pulse shaper with amplitude arrays being (a) (1, 1, 1, 1, 1, 1, 1, 1), (b) (1, 0.5, 1, 0.5, 1, 0.5, 1, 0.5), (c) (1, 1, 1, 1, 0.5, 0.5, 0.5, 0.5), and (d) (1, 1, 1, 1, 0, 0, 0, 0).

Figure 3 illustrates the schematic diagram of the silicon-integrated pulse shaper based on eight-path FIR. First, three cascaded Y branches divide the input signal (usually an ultrashort pulse with a broadband optical frequency comb) into eight paths. Consequently, the light of each path is modulated by an amplitude modulator assisted by optical force. Then, each optical path has an incremental time delay of 10 ps. Finally, the cascaded Y branches combine all light beams from the eight paths. The transfer function of the optical pulse shaper can be described by

$$H(f) = \sum_{n=1}^{8} \alpha_n \mathrm{e}^{\mathrm{j}(2\pi f \cdot n\tau}, \tag{4}$$

where n is the number of the paths, α the attenuation caused by the amplitude modulator, and τ the time delay. The simulated spectra of the optical pulse shaper with different amplitude arrays (α_1, α_2, α_3, α_4, α_5, α_6, α_7, α_8) are shown in Fig. 4, where figures 4(a)–4(d) are for the simulated spectra when the amplitude arrays are set to be (1, 1, 1, 1, 1, 1, 1, 1), (1, 0.5, 1, 0.5, 1, 0.5, 1, 0.5), (1, 1, 1, 1, 0.5, 0.5, 0.5, 0.5), and (1, 1, 1, 1, 0, 0, 0, 0), respectively. We can see that the output spectrum changes with amplitude setting for each of the eight paths, revealing a pulse shaper. Then we can use this optical pulse shaper to implement arbitrary waveform generation.

Figures 5(a) and 5(b) show the platform and 3D diagram of the amplitude modulator. The cantilever structure is used in one arm of the MZI, and a pump light can be launched into the waveguide to adjust the total phase variation. To ensure that the phase difference between the two arms is an integral multiple of 2π when the pump power is zero, we divide the cantilever structure into three parts as shown in Fig. 5(c). The length of the first part is 30 μm and its effective refractive index is 2.371, and the lengths of the second and third part are 90 μm and 15.55 μm respectively. And the effective refractive indexes of the second and third parts are 2.338 and 2.335 respectively.

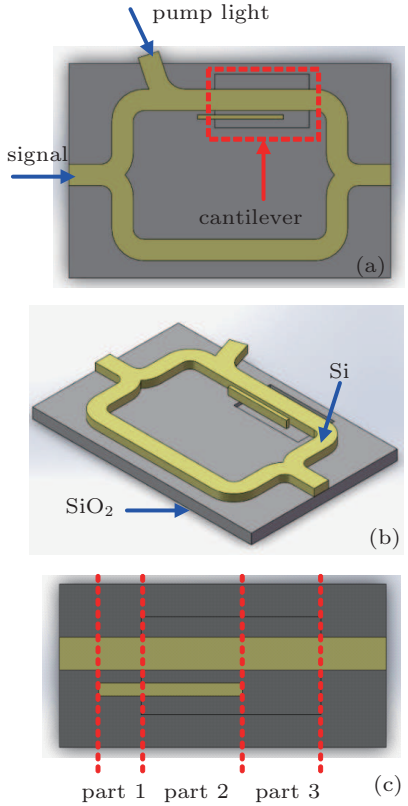


Fig. 5. (color online) (a) platform and (b) 3D diagram of the amplitude modulator using optical force, (c) three parts of the cantilever structure.

The pulse shaper then can be used to generate arbitrary waveforms. Taking triangular waveform for example, we should adjust the amplitude modulator to make the transmission of each path with triangular shape, which is shown in Fig. 6(a) (solid square). The pump power for each path is also shown (solid circle) while ignoring the influence of the signal light. Since the pump power is at a sub-milliwatt level, we should consider the influence of the power of signal light. According to Fig. 2(d), the phase caused by signal light is less than 180° if the signal power is lower than 0.656 mW in each path. Generally, we can control the signal power in each path to be less than 0.25 mW to eliminate the impact of signal power. Even so, the amplitude modulator can realize 360° phase shift, so the influence of the signal power can be compensated for by pump light. Figure 6(b) shows the simulated output spectrum and waveform of the pulse shaper, and the ideal spectrum and waveform of triangular waveform are also shown for comparison. The simulated spectrum is a periodic function, whose spectrum in one period accords well with the ideal one. We use a bandpass filter to filter out one period of the simulated spectrum and use the inverse Fourier transform to calculate the output temporal waveform. We find that the simulated waveform also accords well with the ideal one.

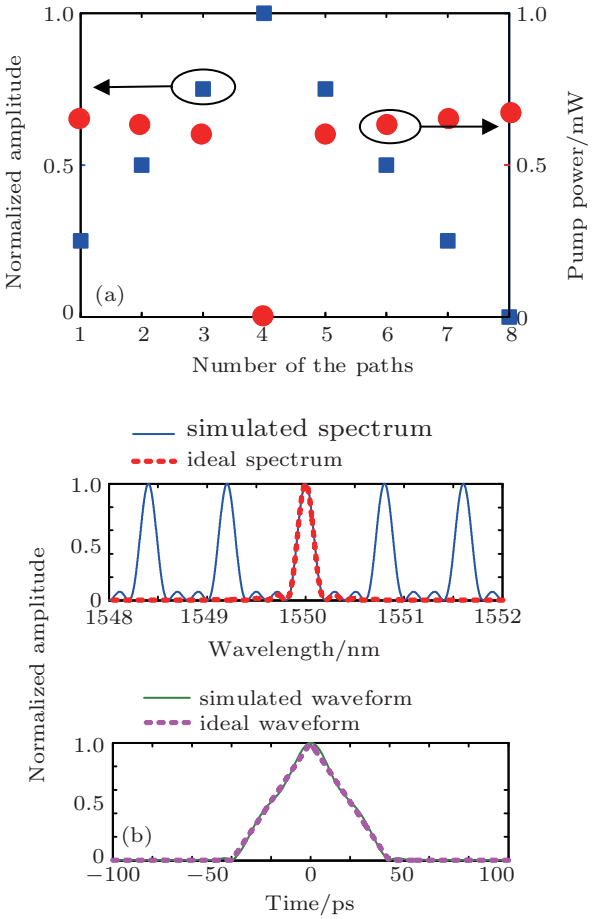


Fig. 6. (color online) (a) Amplitude (solid square) and pump power (solid circle) of each path to generate a triangular waveform, (b) simulated spectrum and waveform of the scheme and the ideal spectrum and waveform of triangular waveform.

To demonstrate the ability to generate arbitrary waveforms, figure 7 shows the generation of several typical waveforms. For example, figure 7(a) illustrates the spectrum and waveform of a rectangular waveform. As only eight taps of FIR are used, the synthesis waveform has a little distortion due to the loss of high frequency components. Figures 7(b)–7(d) show the waveforms of sawtooth shape, Gaussian shape, and raised cosine shape, respectively. These generated waveforms are all in good agreement with the ideal ones.

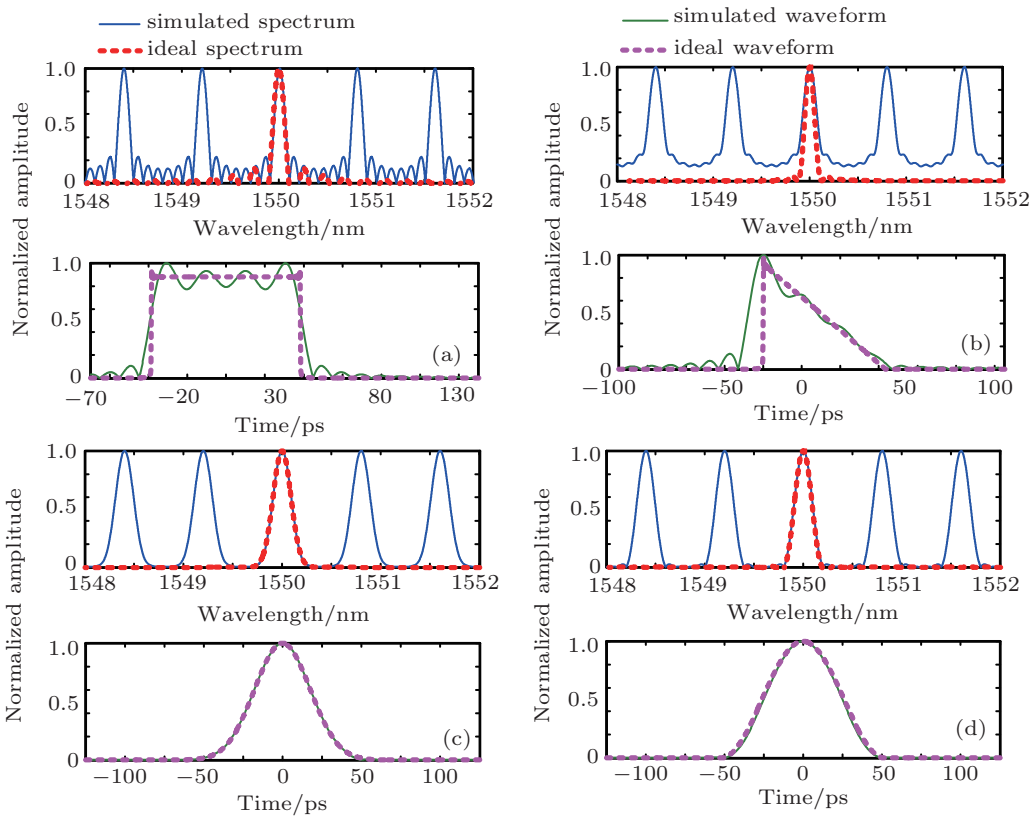


Fig. 7. (color online) Simulated results compared with the ideal ones of (a) square waveform, (b) sawtooth waveform, (c) Gaussian waveform and, (d) raised cosine waveform.

It should be noted that the cantilever structure design and the simulation are both under ideal conditions. The fabrication error and the imperfect input signal may deteriorate the performance of the output waveform. The uneven loss of each path, uneven splitting ratio of Y branch may cause output waveform to be distorted. However, we can pre-compensate for the uneven amplitude by the amplitude modulator on each path to achieve the ideal waveform. In terms of time delay error in each path, the output waveform will be distorted to some extent. In practical fabrication process, the time delay error should be below 2%. Thus the influence induced by the error of time delay can be ignored.

3. Conclusions

We proposed an on-chip optical pulse shaper with eight-tap FIR. The amplitude modulator of each tap is implemented by a new manipulation degree of freedom, i.e., optical force. The pulse shaper has low power consumption due to low pump power of sub-milliwatt level. We further studied the phase variation with the pump power and simulated the generation of several typical waveforms, such as triangular pulse, sawtooth pulse, Gaussian pulse, and raised cosine pulse. Our scheme has advantages in compactness, capability for integrating electronics and fabricating a homogenous silicon chip. Our scheme is based on manipulation of optical force, so no microelectrodes are required on the silicon chip to make the device process much simpler.

References

[1] Weiner A W 2011 *Opt. Commun.* **284** 3669
[2] Fang X, Wang D N and Li S 2003 *J. Opt. Soc. Am. B* **20** 1603
[3] Khan M H, Shen H, Xuan Y, Zhao L, Xiao S, Leaird D E, Weiner A M and Qi M 2010 *Nat. Photo.* **4** 117
[4] Dugan M, Tull J and Warren W 1997 *J. Opt. Soc. Am. B* **14** 2348
[5] Monsterleet A, Tonda-Goldstein S, Dolfi D, Huignard J, Sapé P and Chazelas J 2005 *Electron. Lett.* **41** 332
[6] Shen M and Minasian R A 2004 *IEEE Photon. Technol. Lett.* **16** 1155
[7] Jiang Z, Leaird D E and Weiner A M 2005 *Opt. Express* **13** 10431
[8] Bortnik B, Poberezhskiy I Y, Chou J, Jalali B and Fetterman H R 2006 *J. Lightwave Technol.* **24** 2752

[9] Huang C B, Leaird D E and Weiner A M 2007 *Opt. Lett.* **32** 3242
[10] Dai Y, Chen X, Ji H and Xie S 2007 *IEEE Photon. Technol. Lett.* **19** 1916
[11] Supradeepa V, Leaird D E and Weiner A M 2009 *Opt. Express* **17** 25
[12] Miao H, Leaird D E, Langrock C, Fejer M M and Weiner A M 2009 *Opt. Express* **17** 3381
[13] Supradeepa V, Leaird D E and Weiner A M 2009 *Opt. Express* **17** 14434
[14] Kuo F M, Shi J W, Chiang H C, Chuang H P, Chiou H K, Pan C L, Chen N W, Tsai H J and Huang C B 2010 *IEEE Photon. J.* **2** 719
[15] Wang C and Yao J 2010 *J. Lightwave Technol.* **28** 1652
[16] Zhang A and Li C 2012 *Opt. Express* **20** 23074
[17] Fontaine N, Scott R, Cao J, Karalar A, Jiang W, Okamoto K, Heritage J, Kolner B and Yoo S 2007 *Opt. Lett.* **32** 865
[18] Jiang W, Soares F M, Seo S W, Baek J H, Fontaine N K, Broeke N K, Cao J, Yan J, Okamoto K and Olsson F 2008 in: *National Fiber Optic Engineers Conference, Optical Society of America*, 2008, p. JThA39
[19] Scott R, Fontaine N, Yang C, Geisler D, Okamoto K, Heritage J and Yoo S 2008 *Opt. Lett.* **33** 1068
[20] Geisler D J, Fontaine N K, He T, Scott R P, Paraschis L, Heritage J P and Yoo S 2009 *Opt. Express* **17** 15911
[21] Shen H, Fan L, Varghese L T, Leaird D E, Weiner A M and Qi M 2010 in: *Conference on Lasers and Electro–Optics*, Optical Society of America, 2010, p. CMS2
[22] Guo X, Zou C L, Ren X F, Sun F W and Guo G C 2012 *Appl. Phys. Lett.* **101** 071114
[23] Long Y, Wang J, Li X, Zhu L, Gui C, Zhang Z and Du J 2013 in: *IEEE Photonics Conference* (IPC), 2013 p. 339
[24] Rakich P T, Popovic M A and Wang Z 2009 *Opt. Express* **17** 18116
[25] Ma J and Povinelli M L 2011 *Opt. Express* **19** 10102